

Toward A Reconfigurable Quantum Network Enabled by a Broadband Entangled Source

ERIC Y. ZHU,^{1,*} COSTANTINO CORBARI,² ALEXEY GLADYSHEV,³
PETER G KAZANSKY,² HOI-KWONG LO,^{1,4} AND LI QIAN^{1,5}

¹*Dept. of Electrical and Computer Engineering, University of Toronto, 10 King's College Rd., Toronto, ON M5S 3G4, Canada*

²*Optoelectronics Research Centre, University of Southampton, SO17 1BJ, United Kingdom*

³*Fiber Optics Research Center of the Russian Academy of Sciences, 119333, 38 Vavilov street, Moscow, Russia*

⁴*Dept. of Physics, University of Toronto, 60 St. George St., Toronto, ON M5S 1A7, Canada*

*eric.zhu@utoronto.ca

⁵l.qian@utoronto.ca

Abstract: We present a proof-of-principle experimental demonstration of a reconfigurable entanglement distribution scheme utilizing a poled fiber-based source of broadband polarization-entangled photon pairs and dense wavelength-division multiplexing (DWDM). The large bandwidth (> 90 nm centered about 1555 nm) and highly spectrally-correlated nature of the entangled source can be exploited to allow for the generation of more than 25 frequency-conjugate entangled pairs when aligned to the standard 200-GHz ITU grid. In this work, 3 frequency-conjugate entangled pairs are used to demonstrate quantum key distribution (QKD), with wavelength-selective switching done manually. The entangled pairs are delivered over 40 km of actual fiber, and an estimated secure key rate of up to 20 bits/s per bi-party is obtained.

© 2019 The authors

1. Introduction

Quantum key distribution (QKD) offers, in principle, an unconditionally secure method for two parties to generate a private cryptographic key. Many point-to-point (PTP) demonstrations using weak-coherent source-based [1] and entanglement-based [2, 3] quantum-cryptographic protocols such as the vaunted BB84 [4], BBM92 [5] and E91 [6] (respectively) have been demonstrated. However, PTP connections do not provide an efficient method to connect multiple users, and efforts thusfar in extending PTP links into multi-user networks have proven to be cumbersome at best.

To that end, QKD networks based upon the hub-and-spoke model, where many end-users can be connected to a trusted node [7–10], are used. Should any one end-user wish to communicate with another user secretly, a random secret key is first generated at the node, then QKD is performed between the node and each user separately; finally, the key is sent to each end-user classically using the QKD key material as a one-time pad. However, the trust model for such a network topology is inherently problematic, as any security vulnerability at the node will compromise the entire network. Additionally, time-multiplexing is often required in such circumstances to service multiple users [11, 12], and only one end-user can perform QKD with the central node at a time.

Other schemes [13, 14] involving wavelength-division multiplexing (WDM) have been introduced where individual users on a PTP network can perform QKD with one another simply by addressing each other at different laser wavelengths. All users are equivalent on the network, and no central trusted node is required. However, each user must have both single photon detectors and laser sources at their disposal, and the incremental cost of adding a new user to an N -user network requires increasing the number of laser wavelengths available to each user to

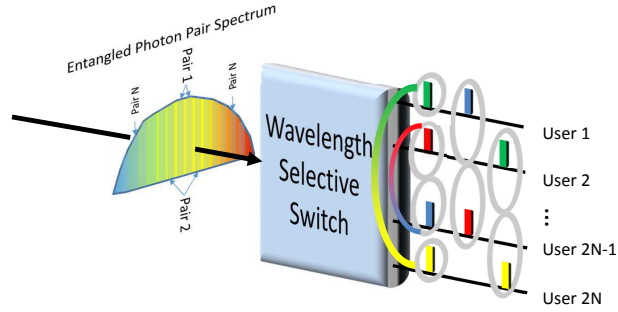


Fig. 1. The use of a broadband entangled source and a wavelength-selective switch (WSS) allows for any two parties on the network to receive frequency-conjugate polarization-entangled photon pairs. The different figure-eights denote the use of different frequency-conjugate pairs to distribute entanglement to different users. The broadband nature of the source also allows for multiple simultaneous connections.

$N + 1$.

In contrast, we show that a reconfigurable quantum network utilizing the distribution of polarization-entangled photon pairs from a (potentially untrustworthy) central office can be realized efficiently using a single broadband entangled source (Fig. 1). While previous works [15–17] have demonstrated the distribution of polarization-entangled photon pairs at distances up to 50 km of fiber using WDM technology, the entangled sources used in those cases left much to be desired. The generation of entangled photon pairs relied upon interferometric methods in [16, 17] which added to experimental complexity, or were limited in both bandwidth [15, 17] (to around 10 nm) and quality of entanglement (raw entanglement fidelity $F < 0.94$). Meanwhile, the fiber-based source [18, 19] used in this work has a bandwidth of over 90 nm, with a quality of entanglement that remains undiminished ($F > 0.98$) over the entire band.

Due to this large bandwidth, the polarization-entangled photon pairs from our source are also highly spectrally-anticorrelated, which allows for multiple (N) frequency-conjugate pairs to be carved out of the spectrum and distributed to N pairs of users simultaneously. When 200-GHz-spacing dense WDM (DWDM) filters are used, $N = 25$ is achievable with our source. With a $2N \times 2N$ wavelength-selective switch (WSS) to perform dynamic spectrum allocation [20], and without additional hardware resources, any user on the network can perform QKD with any other user. Additionally, our scheme allows multiple users ($2N$) to perform QKD simultaneously; when combined with time-multiplexing, such a scheme can extend the number of (non-simultaneous) users well beyond $2N$.

As a proof of principle, we choose 3 frequency-conjugate pairs out of the 25 to demonstrate this entanglement distribution idea. With two single-photon detectors at our disposal (one detector for Alice, the other for Bob), filter pairs are swapped manually to demonstrate dynamic wavelength allocation.

2. Experimental scheme

In this section, we first provide an overview of the entangled source, the poled optical fiber, followed by a description of the experimental setup used for entanglement distribution and QKD.

The source of polarization-entangled photon pairs (PEPPs) used in this work is based upon the poled optical fiber [21, 22]. It is a step-index fiber composed of fused silica glass that exhibits a non-zero second-order nonlinearity (SON). The SON is induced through the pro-

cess of thermal poling [21], and involves the application of a large DC electric field (kV/ μm) at elevated temperatures (500 K) that breaks the inversion symmetry of the glass by creating a frozen-in electric field [21, 22] E_{DC} ; this field in turn induces a second-order nonlinearity (SON): $\chi_{eff}^{(2)} = 3\chi^{(3)}E_{DC}$ [23]. The poling process is facilitated by the geometry of twin-holed fiber [22], where two air-holes [Fig. 2(a)] run along the length of the fiber and sandwich the fiber core; these holes allow for thin electrodes to be threaded through the length of the fiber to allow for the application of the large DC electric field [Fig. 2(b)]. The non-zero SON in the fiber then enables the generation of photon pairs through the process of spontaneous parametric downconversion (SPDC).

However, while a SON is a necessary ingredient for efficient SPDC, it is not sufficient. Phase-matching between pump and downconverted photon pairs must also be satisfied. This is done by periodically erasing [24] the SON [Fig. 2(c)] along the length of the fiber (at a period of Λ) with ultraviolet (UV) light, which yields a quasi phase-matching (QPM) condition:

$$k(\omega_p) = k(\omega_s) + k(\omega_i) + \frac{2\pi}{\Lambda},$$

where $k(\omega_m)$ is the fiber propagation constant at frequency ω_m , with m being either the pump (p), signal (s), or idler (i). The value of Λ can be judiciously chosen so that the pump, signal, and idler are each at an arbitrary wavelength within the transparency window of the fiber, subject to the energy conservation constraint $\omega_p = \omega_s + \omega_i$. In our case, we choose Λ so that the downconverted signal and idler photons are generated in the 1.5-micron telecom band. After periodic UV erasure, the uniformly-poled twin-holed optical fiber has now become a periodically-poled silica fiber (PPSF). We will use PPSF and ‘poled fiber’ interchangeably in the remainder of the text.

The presence of a type-II phasematching [23] and the extremely low birefringence of the fiber (< 10 fs/m) allow for the direct generation of PEPPs [25] in the triplet state

$$|\Psi^+\rangle = \frac{1}{\sqrt{2}} (|HV\rangle + |VH\rangle).$$

Additionally, due to the low group velocity dispersion of the poled fiber, PEPPs can be generated over an extremely broad band of more than 90 nm [18, 19] without significant reduction in the quality of polarization entanglement.

A modified regeneratively-modelocked Ti:Sapphire laser (Spectra-Physics Tsunami) set to 777.45 nm and stabilized with an intracavity interference filter is used to pump the poled fiber with a 81.6 MHz train of 400-ps-long pulses; the average power inside the poled fiber is approximately 50 mW. The broadband spectral correlations [18] (Fig. 3) of the source are employed to distribute multiple frequency-conjugate pairs centered about 1554.9 nm ($= 2 \times 777.45$ nm) to different parties. This central wavelength also happens to coincide with Channel 28 of the ITU DWDM grid [26].

Figure 3 shows the joint-spectral intensity (JSI) of the downconverted photon pairs from the poled fiber. The measurement of the JSI was obtained with a fiber spectrometer [27, 28]. Due to the highly spectrally-anticorrelated nature of the downconverted photons, many frequency-conjugate pairs can be obtained simultaneously using dense wavelength division multiplexing (DWDM) technology.

In Table 1, the figures of merit (tangle, fidelity) of the polarization entanglement for three frequency-conjugate pairs (with signal-idler separation varying from 3 nm, 45 nm, and 75 nm) are given. The three wavelength pairs were chosen not only to demonstrate the large bandwidth of the source, but also to show that the quality of entanglement is consistently high over the entire band. The values in Table 1 were obtained by performing quantum state tomography at a pair generation rates of approximately 4×10^{-3} pairs/pulse/nm using DWDM filters with 1

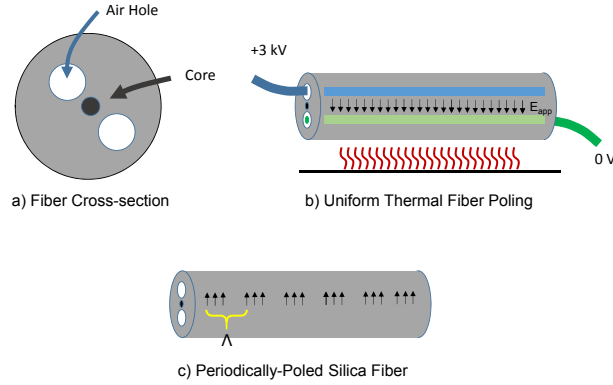


Fig. 2. (Color online) a) Cross-section of a twin-hole fiber used for thermal poling. Two large air holes sandwich the fiber core. b) The thermal poling process. Electrodes are threaded through the air holes, and a large DC potential (E_{app}) is applied across them while the fiber is heated. After the poling process, the electrodes are removed, and a frozen in electric field E_{DC} (whose polarity is opposite to the poling field E_{app}) is created along the length of the fiber. c) Quasi phase-matching is achieved by periodically erasing the E_{DC} (and consequently, the SON) along the length of the fiber with UV light. The fiber is now a periodically-poled silica fiber (PPSF).

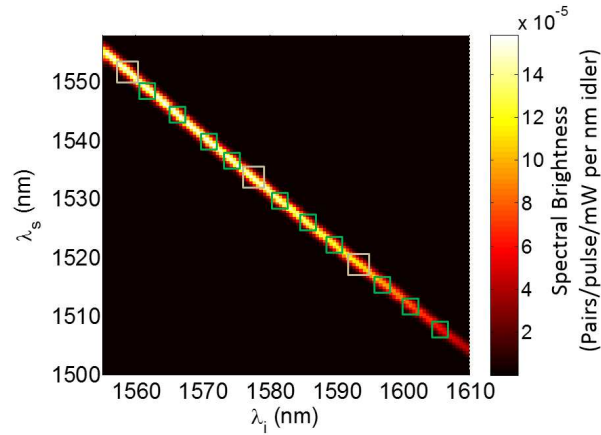


Fig. 3. (Color online) The joint spectral intensity (JSI) of the downconverted photons is plotted as a function of the signal and idler wavelength. A total of 6.8×10^{-3} pairs/pulse per mW of average pump power is generated over the entire spectrum. We observe that the JSI is extremely spectrally-anticorrelated. This anti-correlation allows us to separate the spectrum into many frequency-conjugate pairs (green and white square boxes). The three pairs used in this work are highlighted by larger white boxes. See Table 1 for the central wavelengths of each pair.

nm bandwidths. Each of these pairs is highlighted in Fig. 3 with a white box. While only 3 distinct conjugate pairs are used here, more than 25 bi-parties can be accommodated inside this downconversion bandwidth of the poled-fiber, assuming channel spacings of 200 GHz that are locked to the ITU grid [26]. An even greater number of biparties can be accommodated when the channel spacings are further reduced to 100 or 50 GHz.

In our proof-of-principle demonstration of multi-user QKD, the experimental setup shown in

Table 1. Polarization Entanglement Figures of Merit

λ_s (nm)	1553.3	1533.3	1518.7
λ_i (nm)	1556.6	1577.1	1593.0
Tangle	0.967 ± 0.002	0.964 ± 0.004	0.952 ± 0.008
Fidelity to Ψ^+	0.989 ± 0.001	0.989 ± 0.001	0.985 ± 0.002

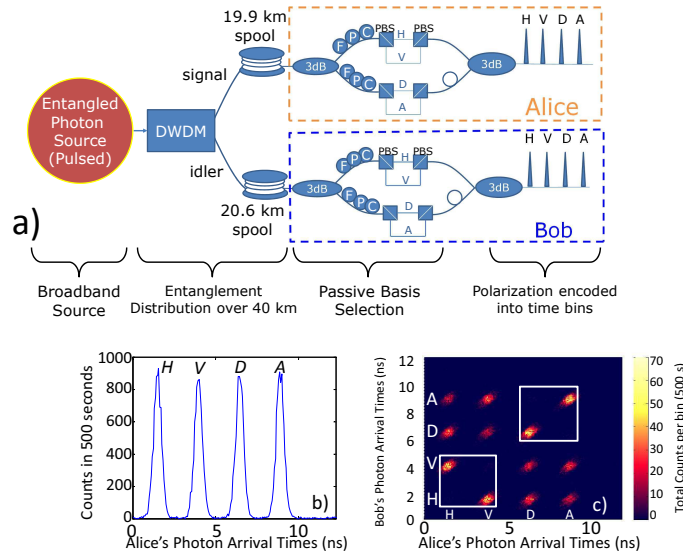


Fig. 4. (a) The full experimental setup for QKD. The signal and idler photons are separated in wavelength by a DWDM filter before they each traverse a 20-km fiber spool and arrive at Alice and Bob's polarization analyzers. (b) During a QKD experiment, Alice tabulates the number of detector 'clicks' she receives as a function of their arrival times (with respect to the pump laser sync signal). (c) A two-dimensional histogram displaying all the coincidence counts observed between Alice and Bob. In a real QKD implementation, only the counts for which Alice and Bob's bases coincided would be kept; these regions are highlighted by square boxes. The data shown in (b) and (c) are obtained when the signal/idler WDMs are centered about 1553.3/1556.65 nm, and a pair generation of 8.9×10^{-3} pairs/pulse. The resolution of the histogram is 64 ps.

Fig. 4(a) is used. A cascaded set of DWDMs is employed to spectrally separate the signal from the idler. Each photon then traverses a 20 km spool of SMF-28 before reaching the polarization analyzers. The BBM92 [5] protocol is implemented, and experiments are run with three different frequency-conjugate signal/idler wavelength pairs (Table 2).

Switching between the various sets of frequency-conjugate filters is done manually, with all other conditions (such as the fiber spans, detectors, pump power, and pump wavelength) kept the same; this allows us to make a meaningful performance comparison between the various wavelength pairs used. The use of a wavelength-selective switch would be a trivial addition to the scheme.

All three filter sets used have very steep cut-on and cut-off wavelengths (> 17 dB/nm), and allow for more than 30 dB extinction between adjacent DWDM channels, meaning crosstalk between adjacent quantum DWDM channels would be negligible. The polarization-dependent

loss for each DWDM is also negligible (< 0.1 dB), as is the polarization mode dispersion (PMD < 0.1 ps); this means that the polarization entanglement of the photon pairs does not degrade after passing through these filters.

Table 2. QKD Experimental Parameters and Results

λ_s (nm)	1553.3	1533.3	1518.7
λ_i (nm)	1556.6	1577.1	1593.0
Pairs/pulse			
Generated per channel	8.9×10^{-3}	7.6×10^{-3}	5.2×10^{-3}
System Loss			
Signal+Idler: (dB)	19.4+19.5	18.7+19.8	18.7+20.7
Sifted Key			
Rate (bits/s) ($\pm 3\sigma$)	32.5 ± 0.7	29.4 ± 0.7	16.3 ± 0.5
QBER ($\pm 3\sigma$):			
e_H (%)	2.35 ± 0.51	1.68 ± 0.45	4.72 ± 1.0
e_D (%)	2.15 ± 0.48	2.23 ± 0.51	7.22 ± 1.2
Secure Key			
Rate (bits/s) ($\pm 3\sigma$)	20.5 ± 1.0	19.7 ± 1.0	4.0 ± 0.9

Each polarization analyzer used in the experiment (Fig. 4a) consists of a 50/50 (3 dB) beam splitter that passively selects the basis in which the photon will be measured. Passive basis selection is used here to reduce the complexity of the system and allow for higher speeds, in comparison to active basis selection. In the top arm of the analyzer, the H/V basis is measured with an unbalanced Mach-Zehnder interferometer (MZI) built from two fiber-pigtailed polarizing beam splitters (PBS); this allows for a time-multiplexed measurement scheme in which a V -polarized photon will arrive 2.5 ns later than an H -polarized photon [18]. A fiber-based polarization controller (FPC) is placed before the PBS-MZI to allow for proper polarization alignment. In the lower arm of the analyzer, a similar unbalanced MZI setup is used to measure the photon in the D/A basis. The two arms are then recombined (at a loss penalty of 3 dB) so that all measurement outcomes $H/V/D/A$ can be discriminated in time and measured by a single detector (the idQuantique id220 free-running single photon detector [SPD]) for each party. This results in the mapping of the polarization degree-of-freedom onto timebins that are evenly-spaced by 2.5 ns [Fig. 4(b)].

An electronic synchronization ('sync') signal derived from the pump laser is used as the global timing reference. A commercial time-to-digital converter, the PicoQuant HydraHarp 400, running in time-tagged T3 mode, is used to generate a two-dimensional histogram, which graphically tallies the coincidence detections as a function of signal (Alice) and idler (Bob)

arrival times [Fig. 4(c)] with respect to the sync signal. This is done at a resolution of 64 ps. For each party, measurements are then binned [Fig. 4(b)] into 1-ns-wide time slots corresponding to the 4 measurement outcomes (H , V , D , and A).

3. Results and Discussion

Table 2 summarizes the results of representative QKD experiments performed for the 3 different frequency-conjugate pairs. The acquisition time T_{acq} for each set of data is 500 seconds.

The estimated QBER (quantum bit error rate) is calculated from the histogrammed data [Fig. 4(c)]. As an example, the QBER in the H/V basis is calculated using the formula:

$$e_H = \frac{C_{H,H} + C_{V,V}}{C_{H,H} + C_{V,V} + C_{V,H} + C_{H,V}}, \quad (1)$$

where C_{P_A, P_B} is the number of coincidence counts observed when Alice and Bob measure in the P_A and P_B polarizations (respectively).

The sifted key rate R_{sif} is calculated using the formula:

$$R_{\text{sif}} = \frac{C_{H,V} + C_{V,H} + C_{D,D} + C_{A,A}}{T_{\text{acq}}}. \quad (2)$$

We note that a bit-flip must be performed for the H/V coincidences [Fig. 4(c), bottom left corner] to account for the anti-correlated outcomes when the Bell state $|\Psi^+\rangle$ is used for QKD.

The secure key rate R_{sec} is estimated from the formula [29]:

$$R_{\text{sec}} = R_{\text{sif}} \left(1 - \frac{1}{2} [h(e_H^u) + h(e_D^u)] - \frac{1}{2} [f(e_H)h(e_H) + f(e_D)h(e_D)] \right), \quad (3)$$

where the factor of $\frac{1}{2}$ is due to the passive basis selection being unbiased, $h(x)$ is the binary Shannon entropy ($h(x) = -x \log_2(x) - (1-x) \log_2(1-x)$), e_H^u (e_D^u) is the upper bound for the QBER in the H/V (D/A) basis used to estimate the number of keys lost due to privacy amplification [30], and $f(e)$ (≥ 1 , but taken to be 1.2 hereafter) is a measure of the efficiency of the error-correcting codes [31].

Finite key analysis is summarized in Table 2, with the values of QBER and R_{sec} accompanied by their uncertainties at 3 standard deviations ($\pm 3\sigma$). If we assume the fair-sampling assumption holds, a low QBER is enough to ensure the security of the key given an untrustworthy central office [29].

The temporal stability of the system is also tested. Using the 1533/1577 frequency-conjugate set, the QKD system is allowed to run many times over the course of two hours (7200 seconds), with no adjustments made to the system over this time. The QBER ($\pm\sigma$) in each run is measured and plotted in Fig. 5; the horizontal error bars represent the acquisition time T_{acq} (≈ 500 s) of the run. We observe that over the course of two hours, the QBER does not change dramatically, implying that the polarization does not drift significantly in a tabletop laboratory setting even over a 40 km spool of fiber with no active polarization stabilization. A total sifted key of 59.4 kbits and an estimated secure key size (Eqn. 3) of 31.2 kbits is generated after this two-hour time period.

We observe (Table 2) that secure key rates of up to 20.5 bits/s can be generated. This key rate, however, can be significantly improved upon if:

- Alice and Bob each have a second detector, with one detector measuring in the H/V basis and the other detector the D/A basis ($\times 4$),
- fiber splice losses due to poled-fiber and other fiber-coupled devices were reduced ($\times 4$),

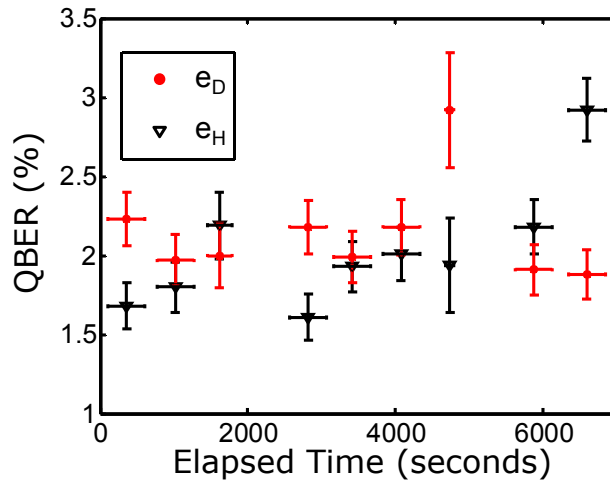


Fig. 5. Time evolution of the QBER for the 1533/1577 signal/idler set. The horizontal errorbars denote the acquisition time for each run (usually 500 seconds), while the vertical bars represent the QBER uncertainty (1 standard deviation) due to statistical fluctuations.

- the detector efficiencies were to increase from the current $\sim 20\%$ to 60% ($\times 9$) by utilizing practical avalanche-photodiode (APD)-based SPDs [32, 33], and
- the pump laser repetition rate were increased from 81.6 MHz to 2 GHz ($\times 25$), generating photon pairs that can be detected using low-deadtime APD-based self-differencing [32] or harmonically-gated [33] SPDs.

These improvements would result in a 3600-fold enhancement of the secure-key rate to 75 kbits/s for each signal/idler channel, or an aggregate 1.5 Mbits/s when the entire spectrum of the poled fiber is utilized. In addition, the strong spectral correlations of our entangled source (Fig. 3) can be exploited for high-dimensional QKD [34], with such a scheme enabling the generation of many more than 1 secure bit per coincidence detection [35].

In summary, we have described a scheme for the distribution of broadband entangled photon pairs to multiple users using standard DWDM wavelength channels. A proof-of-principle QKD experiment for this scheme was performed, yielding estimated secure key rates of up to 20 bits/s per channel. This brings us a step closer toward an entanglement-based, reconfigurable multi-user quantum network that is compatible (without additional resources) to current optical network infrastructures.

Funding

We acknowledge the Natural Sciences and Engineering Research Council (Canada) and the EU Project CHARMING (Contract No. FP7-288786) for funding the work presented in this paper.

References

1. T. Schmitt-Manderbach, H. Weier, M. Fürst, R. Ursin, F. Tiefenbacher, T. Scheidl, J. Perdigues, Z. Sodnik, C. Kurtsiefer, J. G. Rarity, A. Zeilinger, and H. Weinfurter, "Experimental demonstration of free-space decoy-state quantum key distribution over 144 km," *Phys. Rev. Lett.* **98**, 010504 (2007).
2. R. Ursin, F. Tiefenbacher, T. Schmitt-Manderbach, H. Weier, T. Scheidl, M. Lindenthal, B. Blauensteiner, T. Jennewein, J. Perdigues, P. Trojek *et al.*, "Entanglement-based quantum communication over 144 km," *Nature physics* **3**, 481–486 (2007).

3. A. Treiber, A. Poppe, M. Hentschel, D. Ferrini, T. Lorünser, E. Querasser, T. Matyus, H. Hübel, and A. Zeilinger, "A fully automated entanglement-based quantum cryptography system for telecom fiber networks," *New Journal of Physics* **11**, 045013 (2009).
4. C. H. Bennett, G. Brassard *et al.*, "Quantum cryptography: Public key distribution and coin tossing," in "Proceedings of IEEE International Conference on Computers, Systems and Signal Processing," , vol. 175 (New York, 1984), vol. 175.
5. C. H. Bennett, G. Brassard, and N. D. Mermin, "Quantum cryptography without bell's theorem," *Phys. Rev. Lett.* **68**, 557–559 (1992).
6. A. K. Ekert, "Quantum cryptography based on bell's theorem," *Phys. Rev. Lett.* **67**, 661–663 (1991).
7. C. Elliott, "Building the quantum network," *New Journal of Physics* **4**, 46 (2002).
8. M. Peev, C. Pacher, R. Alleaume, *et al.*, "The SECOQC quantum key distribution network in Vienna," *New Journal of Physics* **11**, 075001 (2009).
9. M. Sasaki, M. Fujiwara, H. Ishizuka, W. Klaus, K. Wakui, M. Takeoka, S. Miki, T. Yamashita, Z. Wang, A. Tanaka, K. Yoshino, Y. Nambu, S. Takahashi, A. Tajima, A. Tomita, T. Domeki, T. Hasegawa, Y. Sakai, H. Kobayashi, T. Asai, K. Shimizu, T. Tokura, T. Tsurumaru, M. Matsui, T. Honjo, K. Tamaki, H. Takesue, Y. Tokura, J. F. Dynes, A. R. Dixon, A. W. Sharpe, Z. L. Yuan, A. J. Shields, S. Uchikoga, M. Legré, S. Robyr, P. Trinkler, L. Monat, J.-B. Page, G. Ribordy, A. Poppe, A. Allacher, O. Maurhart, T. Länger, M. Peev, and A. Zeilinger, "Field test of quantum key distribution in the tokyo qkd network," *Opt. Express* **19**, 10387–10409 (2011).
10. R. J. Hughes, J. E. Nordholt, K. P. McCabe, R. T. Newell, C. G. Peterson, and R. D. Somma, "Network-centric quantum communications with application to critical infrastructure protection," arXiv preprint arXiv:1305.0305 (2013).
11. I. Choi, R. J. Young, and P. D. Townsend, "Quantum information to the home," *New Journal of Physics* **13**, 063039 (2011).
12. B. Fröhlich, J. F. Dynes, M. Lucamarini, A. W. Sharpe, Z. Yuan, and A. J. Shields, "A quantum access network," *Nature* **501**, 69–72 (2013).
13. W. Chen, Z.-F. Han, T. Zhang, H. Wen, Z.-Q. Yin, F.-X. Xu, Q.-L. Wu, Y. Liu, Y. Zhang, X.-F. Mo, Y.-Z. Gui, G. Wei, and G.-C. Guo, "Field experiment on a star type metropolitan quantum key distribution network," *Photonics Technology Letters, IEEE* **21**, 575–577 (2009).
14. S. Wang, W. Chen, Z.-Q. Yin, Y. Zhang, T. Zhang, H.-W. Li, F.-X. Xu, Z. Zhou, Y. Yang, D.-J. Huang, L.-J. Zhang, F.-Y. Li, D. Liu, Y.-G. Wang, G.-C. Guo, and Z.-F. Han, "Field test of wavelength-saving quantum key distribution network," *Opt. Lett.* **35**, 2454–2456 (2010).
15. C. Autebert, J. Trapateau, A. Orioux, A. Lemaître, C. Gomez-Carbonell, E. Diamanti, I. Zaquine, and S. Ducci, "Multi-user quantum key distribution with entangled photons from an algaas chip," *Quantum Science and Technology* **1**, 01LT02 (2016).
16. H. C. Lim, A. Yoshizawa, H. Tsuchida, and K. Kikuchi, "Wavelength-multiplexed distribution of highly entangled photon-pairs over optical fiber," *Opt. Express* **16**, 22099–22104 (2008).
17. I. Herbauts, B. Blauensteiner, A. Poppe, T. Jennewein, and H. Hübel, "Demonstration of active routing of entanglement in a multi-user network," *Opt. Express* **21**, 29013–29024 (2013).
18. E. Y. Zhu, Z. Tang, L. Qian, L. G. Helt, M. Liscidini, J. E. Sipe, C. Corbari, A. Canagasabay, M. Ibsen, and P. G. Kazansky, "Poled-fiber source of broadband polarization-entangled photon pairs," *Opt. Lett.* **38**, 4397–4400 (2013).
19. C. Chen, E. Y. Zhu, A. Riazzi, A. V. Gladyshev, C. Corbari, M. Ibsen, P. G. Kazansky, and L. Qian, "Compensation-free broadband entangled photon pair sources," *Optics Express* **25**, 22667–22678 (2017).
20. J. Oh, C. Antonelli, and M. Brodsky, "Coincidence rates for photon pairs in wdm environment," *Journal of Lightwave Technology* **29**, 324–329 (2011).
21. P. Kazansky, "Thermally poled glass: frozen-in electric field or oriented dipoles?" *Opt. Commun.* **110**, 611–614 (1994).
22. A. Canagasabay, C. Corbari, A. V. Gladyshev, F. Liegeois, S. Guillemet, Y. Hernandez, M. V. Yashkov, A. Kosolapov, E. M. Dianov, M. Ibsen, and P. G. Kazansky, "High-average-power second-harmonic generation from periodically poled silica fibers," *Opt. Lett.* **34**, 2483–2485 (2009).
23. E. Y. Zhu, L. Qian, L. G. Helt, M. Liscidini, J. E. Sipe, C. Corbari, A. Canagasabay, M. Ibsen, and P. G. Kazansky, "Measurement of $\chi(2)$ symmetry in a poled fiber," *Opt. Lett.* **35**, 1530–1532 (2010).
24. C. Corbari, A. Canagasabay, M. Ibsen, F. Mezzapesa, C. Codemard, J. Nilsson, and P. Kazansky, "All-fibre frequency conversion in long periodically poled silica fibres," in "Optical Fiber Communication Conference, 2005. Technical Digest. OFC/NFOEC," , vol. 5 (OSA, Optical Society of America., 2005), vol. 5.
25. E. Y. Zhu, Z. Tang, L. Qian, L. G. Helt, M. Liscidini, J. Sipe, C. Corbari, A. Canagasabay, M. Ibsen, and P. G. Kazansky, "Direct generation of polarization-entangled photon pairs in a poled fiber," *Phys. Rev. Lett.* **108**, 213902 (2012).
26. "Spectral grids for wdm applications: Dwdm frequency grid," ITU-T Recommendation G.694.1. (2012).
27. M. Avenhaus, A. Eckstein, P. J. Mosley, and C. Silberhorn, "Fiber-assisted single-photon spectrograph," *Opt. Lett.* **34**, 2873–2875 (2009).
28. E. Y. Zhu, C. Corbari, P. Kazansky, and L. Qian, "Self-calibrating fiber spectrometer for the measurement of broadband downconverted photon pairs," arXiv preprint arXiv:1505.01226 (2015).
29. D. Gottesman, H.-K. Lo, N. Lütkenhaus, and J. Preskill, "Security of quantum key distribution with imperfect

- devices,” *Quantum Information and Computation* **4**, 325–360 (2004).
30. N. Lütkenhaus, “Security against individual attacks for realistic quantum key distribution,” *Phys. Rev. A* **61**, 052304 (2000).
 31. G. Brassard and L. Salvail, “Secret-key reconciliation by public discussion,” in “Advances in Cryptology - EUROCRYPT '93,” vol. 765 of *Lecture Notes in Computer Science*, T. Hellesest, ed. (Springer Berlin Heidelberg, 1994), pp. 410–423.
 32. L. Comandar, B. Fröhlich, J. Dynes, A. Sharpe, M. Lucamarini, Z. Yuan, R. Penty, and A. Shields, “Gigahertz-gated ingaas/inp single-photon detector with detection efficiency exceeding 55% at 1550 nm,” *Journal of Applied Physics* **117**, 083109 (2015).
 33. A. Restelli, J. C. Bienfang, and A. L. Migdall, “Single-photon detection efficiency up to 50% at 1310 nm with an ingaas/inp avalanche diode gated at 1.25 ghz,” *Applied Physics Letters* **102**, 141104 (2013).
 34. J. Nunn, L. J. Wright, C. Söller, L. Zhang, I. A. Walmsley, and B. J. Smith, “Large-alphabet time-frequency entangled quantum key distribution by means of time-to-frequency conversion,” *Opt. Express* **21**, 15959–15973 (2013).
 35. T. Zhong, H. Zhou, R. D. Horansky, C. Lee, V. B. Verma, A. E. Lita, A. Restelli, J. C. Bienfang, R. P. Mirin, T. Gerrits *et al.*, “Photon-efficient quantum key distribution using time–energy entanglement with high-dimensional encoding,” *New Journal of Physics* **17**, 022002 (2015).